Journal of
Polymer Materials

Tech Science Press

http://doi.org/10.32604/jpm.2026.082303

ARTICLE

Facile Preparation of TiO_2/PMMA Nanocomposites with Enhanced Physio-Mechanical Properties for Dental Applications

Abdul Hakim Shah[1,*], Hassan Khan[1], Muneerah Alomar[2,*], Atta ur Rahman[1], Muhammad Hanif[3], Salah ud Din[4], Haseena Riffat[1], Nazir ur Rehman[5], Munazza Gul[1], Muhammad Danyal Zarin[1], Muhammad Faran[1], Muhammad Wasim[1] and Aqib Umar[1]

[1]Department of Physics, Khushal Khan Khattak University, Karak, Pakistan
[2]Department of Physics, College of Science, Princess Nourah bint Abdulrahman University, Riyadh, Saudi Arabia
[3]Department of Mechanical Engineering, College of Electrical and Mechanical Engineering (E & ME), National University of Sciences and Technology (NUST), Islamabad, Pakistan
[4]KMU Institute of Pathology and Diagnostic Medicine, Khyber Medical University, Peshawar, Pakistan
[5]Department of Geology, Khushal Khan Khattak University, Karak, Pakistan
*Corresponding Authors: Abdul Hakim Shah. Email: dr.abdulhakim@kkkuk.edu.pk;
Muneerah Alomar. Email: muaalomar@pnu.edu.sa

Received: 13 March 2026; Accepted: 05 June 2026; Published: 24 September 2026

ABSTRACT: Dental caries (or tooth decays) is a common oral disease in early childhood and adults of all ages, which is caused by long-term synergies of acid-producing bacteria and fermentable carbohydrates in the oral environment. The use of existing dental restorative materials (including silver amalgams, light-cured resins, and dental restorative composites) and dental restorative composites (including glass ionomers cement, despite being sealants, releasing fluoride and promoting remineralization) is commercially restricted due to their weak mechanical properties, poor abrasion resistance, low elastic modulus, improper shrinkage, less polishability, brittleness, poor wear resistance tensile strength, aesthetic etc. Therefore, the physical intercalation of nano-fillers with polymer resins in nanocomposites might be a better alternative, mainly due to the high surface area of nanofillers. The present work reports an economical hydro-solvo thermal combinatory method to prepare TiO_2/PMMA nanocomposites with four distinct wt% (3%, 6%, 9% and 12%) of TiO_2 nanofillers. Their comparative structural, morphological, and functional group analysis was carried out with that of pure PMMA by XRD, AFM, and FTIR, respectively. The physio-mechanical properties of the nanocomposites (including Young modulus, ultimate tensile strength, break strength, hardness value (HV), flexural strength, water absorption, density tests and polymerization shrinkage) were measured using UTM, ASTM D790 standard, the Archimedes method and ASTM D570 standard, respectively. Significant enhancement in Young's modulus, ultimate tensile strength, break strength, hardness value (HV), and flexural strength were recorded as compared with that of the pure PMMA, achieving the optimum values (1.23 times in Young's modulus, 2.38 times in UTS, 2.37 times in break strength, and 2 times in HV) for the nanocomposite with 9% TiO_2 nanofiller. Similarly, significant reduction in water adsorption and polymerization shrinkage (linear decrease) was observed with increasing filler (TiO_2) contents, which reveals the dimensional stability of nanocomposites, favorable for dental implants, and this is attributed to the effective bonding of TiO_2 nanoparticles with the PMMA matrix. Such a tremendously enhanced physio-mechanical behavior of the TiO_2/PMMA nanocomposite (particularly with 9 wt% TiO_2 nanofiller) reveals its promising potential for use as a dental restorative material.

KEYWORDS: PMMA; TiO_2; hydro-solvothermal; nanocomposites; optimization; physio-mechanical

1 Introduction

Dental caries, or simply tooth decay, has been considered a severe oral disease in adults of all ages, particularly in 60–90% of school-going children, caused by long-term synergies of acid-producing bacteria and fermentable carbohydrate in the oral environment [1,2]. Many kinds of dental materials have been developed for caries treatment and prevention, which include Silver (in use for more than 150 years) [3,4], light-cured resins, amalgams, etc. [3]. Amalgam is a kind of metallic filler, composed of mercury (nearly 50%) and a powdered alloy (mostly from silver, zinc, etc.). However, the continuous use of silver amalgam for tooth fillings or capping brings toxicity, poor aesthetic nature, odd look, and therefore, it is declared as less feasible for use in restorative dentistry. Alternatively, light-cured resins were adopted as dental restorative materials due to their excellent esthetic, biocompatible, adhesive, manipulative, durability, and their matching ability with the oral cavity environment (such as pH: 4–8, temperature range 0–70°C, the chewing force up to 80 N, and more than seven hundred kinds of existing bacteria) [3–6]. However, their weak mechanical properties, poor abrasion resistance, and relatively low elastic modulus create challenges. Furthermore, the shrinkage ratio of the resin material in the curing process needs to be strongly hindered and fulfill the clinical application along with an increase in restorative efficiency [7]. These drawbacks with the silver amalgams and resin materials led the researchers to explore other materials such as the dental restorative composites (glass ionomers, compomers, resin-based composites, ormocers, etc.) for this purpose [8–10].

Dental restorative composites are generally a homogenous blend of a matrix (relatively soft) and an inorganic filler (a hard one) [1]. The atomic level interactions make them favorable to execute essential dental restorative properties [11,12]. Glass ionomers cement is often used as a filling material in the dental restorative composites, which acts as sealants, releasing fluoride and promoting remineralization [13]. However, as compared to the resin composites, the commercial use of restorative composites is restricted due to certain parametric limitations such as less polishability, brittleness, poor wear resistance and tensile strength etc. by the dental practitioners [13,14].

An alternate choice of material for the dental restorative purposes is polymer based nanocomposites in which the polymer matrix resin is filled with nanomaterials. PMMA resin is a commonly used polymer for optical and biomedical applications. Its selection is based on its unique properties such as high optical clarity and UV resistance, biocompatibility, colour matching, light weight and economical cost [14]. However, certain lacks such as weak wear resistance and poor surface hardness have limited its physio-mechanical properties for dental applications [15].

The introduction of nanomaterials as fillers within the polymer resins is a new strategy to boost up the mechanical properties of nanocomposites for dental applications because the nanomaterials offer high surface area-to-volume ratio, which further enhances their interfacial interaction with the resin matrix [16]. The performance optimization of polymer nanocomposites depends on the type, size, morphology and distribution of incorporated nanomaterial and its interaction with the polymer matrix [17]. The integration of polymers' and fillers' characteristics within the nanocomposites results in enhanced rigidity, toughness, hardness and other performance parameters essential for dental applications. Earlier, MWCNTs [18] and metals/metal oxides nanoparticles including SiO_2 [19], Ag [20], ZrO_2 [21,22] and TiO_2 [23,24] etc. have been investigated as fillers for dental restorative materials to improve their mechanical and physical properties. Likewise, friction-induced PTFE coating (FIPC) technology has been developed, which constructs transfer films by the friction of PTFE balls and applied it in zirconia/silica (ZrO_2/SiO_2) gel filler-modified photocurable composite resin. This FIPC technology, as proclaimed to offer ultralow coefficient of friction (COF: 0.05–0.07) and exhibit long term lubrication stability, has shown some potential for dental restorative

and biomedical coating areas [25]. Similarly, a widespread research is in run since long, to improve the root canal disinfection and accelerate the rate of pulp regeneration, which is done by integrating antibacterial agents into the hydrogel matrix and stimulating an immune response [26]. In an another study, an injectable fast-setting Tricalcium Silicate based material; TCS/β-tricalcium phosphate/monocalcium phosphate anhydrous (β-TCP/MCPA) cement has been developed by the incorporation of hydroxypropyl methylcellulose (HPMC) and β-TCP/MCPA, which have offered some good physio-chemical properties including setting time, anti-washout property, injectability, compressive strength, apatite mineralization and sealing. However, despite that fact of exhibition of these physio-chemical properties, biocompatibility and enhanced osteo/odontogenic differentiation of SHED and high injection rate, the excessive additions of β-TCP/MCPA compromised its injectability and compressive strength [27]. Study of underlying mechanisms and the current clinical therapies of bone metastases highlight the advances of intelligent nanosystems to stimulate vascular regeneration, promote bone regeneration, eliminate tumor cells, minimize bone damage [28]. Most recently, Ti-based metallic glass composites containing β-Ti dendrites were investigated as dental materials [29]. All such investigations reveal that despite of offering significant properties including chemical and thermal stability, bio-compatibility, adequate toxicity and strong surface activity, it is observed that the synthesis methods for polymers based composites are luxurious and there is a room to achieve adequacy in the denture properties [19]. The design of economical methods to prepare polymers based nanocomposites on bulk level and minimize lacks in certain performance parameters such as polymerization shrinkages (PS) and water absorption (WS) level have restricted their commercial usage which is still a challenging task for the researchers. Introduction of inorganic fillers into the resins composites is a way out to solve these issues. The TiO_2 nanofiller is a preferred choice due to its unique anti-bacterial and self-cleaning properties [30,31]. Its blend within the restorative materials improves the mechanical strength, reduce polymerization shrinkage and water sorption [32] while avoiding corrosion and irritation in cavity [33].

In this work, we report a combined hydro-solvo thermal method to prepare TiO_2/PMMA nanocomposites with four distinct wt% TiO_2 nanofillers (3%, 6%, 9% and 12%). The TiO_2 nanoparticles were synthesized hydrothermally, followed by the preparation of their composites with PMMA via a solvothermal approach. Comparative analysis of these nanocomposites was carried out with pure PMMA and TiO_2 for structure, morphology, functional groups, mechanical (Young modulus, density and water absorption tests) and thermal properties (wt% degradation) via XRD, AFM, FTIR, UTM, The Archimedes method, ASTM D570 etc., respectively. Significant enhancement in physio-mechanical properties was observed for nanocomposites (particularly, with 9% TiO_2 filler content), which is attributed to the effective bonding of TiO_2 nanoparticles with the PMMA matrix. Such a tremendous improved behavior reveals its suitability for the use as a best alternate dental restoring material.

2 Materials and Methods

2.1 Materials

The chemicals; Titanium isoproxide "Ti $[OCH(CH_3)_2]_4$", purity 97–99.99%, Sodium hydroxide (NaOH) purity 97%, poly(methyl methacrylate) purity ≥ 99.99% and acetone 99.5–99.9%, were obtained commercially from Sigma Aldrich and other suppliers, which were used without further treatment.

2.2 Methods for the Preparation of TiO_2/PMMA Nanocomposites

A combined hydrothermal and solvothermal method was applied to prepare the nanocomposites as the recent studies have reported that hydrothermal-solvothermal routes enable excellent control over the

morphology of inorganic TiO_2 phase and its interface with the matrix, properties as compared to the conventional *in-situ* polymerization methods [34]. To be more specific, the *in-situ* polymerization mainly delivers the physical encapsulation of interacting particles within a polymer matrix and control over crystallinity, morphology, and interfacial interactions are restricted. While, the combined hydro-solvothermal conditions (pH, reaction time etc.) yields controlled nucleation and growth of the fillers phase under higher temperature and pressure, thereby leads to form highly crystalline structures with varying morphology. Further, the combined hydro-solvothermal approach results in a uniform dispersion and favoring interfacial integration between the matrix and fillers, by maintaining a controlled reaction environment (aqueous in hydrothermal and organic in solvothermal). This results in enhanced physicochemical properties of the product material, not easily realized with simple *in-situ* polymerization.

The whole process is divided into three steps;

Step 1: Synthesis of TiO_2 nanoparticles (Fillers)

TiO_2 nanoparticles were synthesized via a hydrothermal. Briefly, Titanium Isopropoxide (10 mL) was added to 150 mL of deionized water under continuous magnetic stirring at room temperature. The mixture was stirred for 3 h until a transparent Titanium (Ti) based solution was obtained. Subsequently, 5 mL of 7.5 M NaOH solution was added dropwise to adjust the solution to basic conditions, followed by further stirring for 30 min. A whitish, milky Ti based precursor solution (pH ≈ 9) was formed, which was then transferred to a Teflon lined autoclave, sealed and maintained at 160°C for 16 h inside a conventional oven for hydrothermal reaction. After completion, the system was allowed to cool naturally to room temperature overnight. The obtained precipitates were collected and washed three times each with deionized water and ethanol via centrifugation at 2000 rpm. The resulting powders were dried at 80°C for 6 h in air and named as T1 (pure TiO_2).

Step 2: Preparation of pure PMMA

In this step, the solid PMMA granules (2 g) were dispersed in acetone (30 mL) under continuous stirring at room temperature for 10 min. The mixture was subsequently heated heating at 60°C for 2 min to obtain a gel, which was cast into a quartz petri dish and heated at 60°C for further 1 h to allow solvent evaporation. The obtained sample was named as P1.

Step 3: Preparation of TiO_2/PMMA nanocomposites

To prepare the nanocomposites, PMMA (2 g) was first dissolved in 20 mL acetone. Prior to gelation, a dispersion of 0.06 g of TiO_2 nanoparticles, (synthesized as described in step 1) in 10 mL ethanol, was mixed with it. The resulting mixture was stirred for 30 min to obtain a homogeneous dispersion, followed by heating at 60°C for 3 min to induce gel formation. The gel was then cast into a quartz Petri dish and dried at 80°C in air to facilitate solvent evaporation. The obtained sample was marked as PTN-3 (3 wt% TiO_2 in PMMA).

Similarly, three other nanocomposites; PTN-6 (6 wt% TiO_2 in PMMA), PTN-9 (9 wt% TiO_2 in PMMA), and PTN-12 (12 wt% TiO_2 in PMMA) were prepared following the same procedure by incorporating 0.12 g, 0.18 g, and 0.24 g of TiO_2 nanoparticles, respectively, into 2 g of PMMA. Each mixture was processed under identical conditions, including gelation, casting in a quartz Petri dish, and drying at 80°C for solvent evaporation.

The nanocomposites samples prepared in this work, are marked as under;

3% TiO_2/PMMA: PTN-3

6% TiO_2/PMMA: PTN-6

9% TiO_2/PMMA: PTN-9

12% TiO_2/PMMA: PTN-12

2.3 Characterization

Structure and phase identification were carried out using X-ray diffraction (XRD) analysis (X-ray diffractometer, Model JDX-3532, JEOL, Japan) with Cu Kα radiation (λ = 1.54 Å). Surface morphology and roughness were examined by atomic force microscopy (AFM) using a JEOL electron microprobe (Model 733). The Young's modulus was determined through universal testing machine (UTM) analysis (Testometric Inc., UK; 100–500 KN capacity) at the Centralized Resource Laboratory, Energy Centre, UET Peshawar. The surface hardness was evaluated using the Vickers hardness test and the flexural strength (or bending strength) was determined using a three-point bending test in accordance with ASTM D790. Fourier Transform Infrared (FTIR) Spectroscopy was performed to investigate the presence of functional groups and chemical bonding.

For the evaluation of dental-related properties, water absorption tests were conducted in accordance with ASTM D570 at the Advanced Functional Nanomaterials Laboratory, Khushal Khan Khattak University Karak. In addition, density and polymerization shrinkage (PS%) were measured to assess volumetric changes and density variations during the curing process.

3 Results and Discussions

3.1 Structure and Morphology

3.1.1 Structure by XRD Analysis

A comparative structural analysis of PMMA, TiO_2, and their nanocomposites was performed using X-ray diffraction (XRD), and the corresponding patterns are presented in Fig. 1. The XRD pattern of pure PMMA exhibits broad diffraction peaks, positioned at $2\theta \approx 13.2^\circ$, 31.04°, and 41.5°, corresponding to the (111), (112), and (211) planes, respectively. The XRD pattern is indexed well with that of the amorphous poly(methyl methacrylate) (PMMA) [35]. The broadness of these peaks with gradual decrease in intensity at higher diffraction angles further confirm its amorphous structure [36].

In contrast, the diffraction pattern of pure TiO_2 is well matched with the JCPDS card No. 73-1764 [37], corresponding to the anatase phase of TiO_2. Distinct and sharp diffraction peaks observed at $2\theta \approx 25.23^\circ$, 38.9°, 47.7°, 54.1°, and 55.3° are respectively assigned to the (101), (004), (200), (105), and (211) crystallographic planes of tetragonal anatase TiO_2, indicating its high crystallinity. The most intense peak at $2\theta \approx 25.23^\circ$, corresponding to the (101) plane, suggests preferential growth of TiO_2 nanostructures along this plane. Notably, this characteristic anatase (101) peak is clearly observed in all nanocomposite samples (PTN-3, PTN-6, PTN-9, and PTN-12), confirming the successful incorporation of TiO_2 into the PMMA matrix. Additionally, the nanocomposites retain the broad diffraction features of PMMA at $2\theta \approx 13.2^\circ$ and 31.04°, corresponding to the (111) and (112) planes, respectively. These results indicate that TiO_2 is effectively embedded within the polymer matrix without altering its structural characteristics and the amorphous nature of PMMA is preserved.

The average crystallite sizes as evaluated using Scherrer's formula [38], are tabulated as Table 1.

Table 1: Average crystallite size of TiO_2/PMMA nanocomposites.

Sample	Average Crystallite Size (nm)	Sample	Average Crystallite Size (nm)
PTN-3	19.2	PTN-9	20
PTN-6	18.4	PTN-12	21

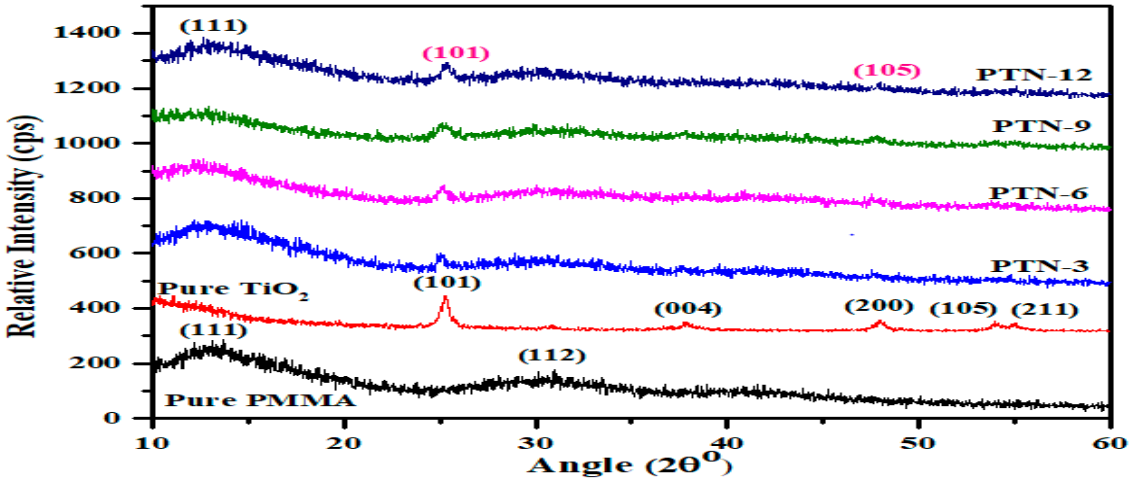

Figure 1: Comparative X-rays diffraction patterns of PMMA and TiO_2/PMMA nanocomposites.

3.1.2 Surface Morphology and Roughness by Atomic Force Microscopy

In order to investigate the surface morphology and surface roughness, atomic force microscopy (AFM) of the pure PMMA and PTNs nanocomposites was performed under ambient conditions (21 ± 1°C and 44 ± 2% relative humidity) using an MFP-3D system (Asylum Research, USA) operating in tapping (intermittent contact) mode. Silicon cantilevers (CSG10, NT-MDT, Russia) with an approximate tip radius of 10 nm and a nominal spring constant of ~0.1 N m^{-1} were employed. All scans were acquired over an area of 5 × 5 μm^2 with a scanning rate of 5 μm/s in forward direction.

To ensure reproducibility, the measurements were conducted four times for each sample at different surface locations. Image processing was limited to first-order plane fitting for background subtraction; no filtering or non-linear treatments (e.g., line-by-line flattening) were applied. The representative three-dimensional AFM topographic and scale images of the pure PMMA and nanocomposites with varying TiO_2 filler contents (0, 3, 6, 9, and 12 wt%) are shown in Fig. 2a–e and Fig. 3a–e, respectively. Surface topography is depicted in three-dimensional perspective, with height information represented by a color scale indicated alongside each image, effectively emphasizing the surface texture. The pure PMMA looks quite flat and smooth, while in the nanocomposite films features appear in the form of TiO_2 nanoparticles, progressively coalescing into connected ridges of increasing width.

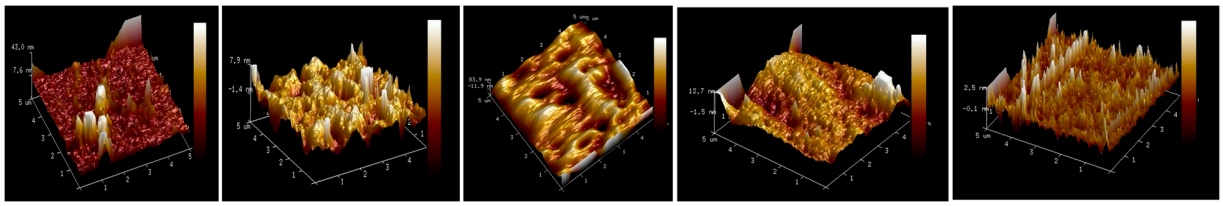

(**a**) (**b**) (**c**) (**d**) (**e**)

Figure 2: AFM topographic images of (**a**) pure PMMA and TiO_2/PMMA nanocomposites with (**b**) 3%, (**c**) 6%, (**d**) 9% and (**e**) 12% TiO_2.

The roughness and texture profiles of pure PMMA and the nanocomposite films were obtained using the Gwyddion software 2.0 and the corresponding curves are shown in Fig. 4a–e and Fig. 5a–e, respectively. The corresponding roughness parameters are tabulated as Table 2. The topography shows a granular texture

with uniformly distributed nanoscale features. The relatively low roughness values indicate a smooth and homogeneous surface, which is favorable for the dental restorative properties.

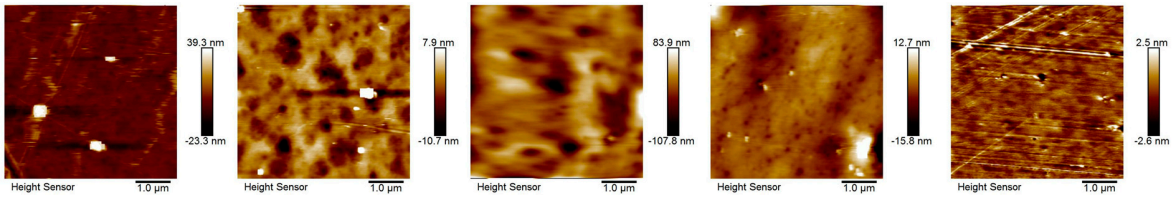

(**a**) (**b**) (**c**) (**d**) (**e**)

Figure 3: Scale AFM images of (**a**) pure PMMA and TiO_2/PMMA nanocomposites with (**b**) 3%, (**c**) 6%, (**d**) 9% and (**e**) 12% TiO_2.

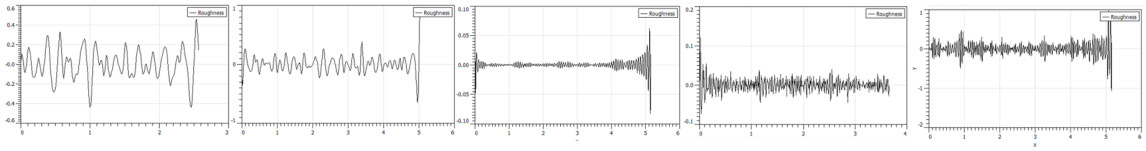

(**a**) (**b**) (**c**) (**d**) (**e**)

Figure 4: The roughness profile extracted from AFM topographic images (**a**) pure PMMA and TiO_2/PMMA nanocomposites with (**b**) 3%, (**c**) 6%, (**d**) 9% and (**e**) 12% TiO_2.

Table 2: AFM parameters for pure PMMA and TiO_2/PMMA nanocomposites.

AFM Parameters	Pure PMMA	PTN-3	PTN-6	PTN-9	PTN-12
Average roughness	0.0569	0.0949	0.01146	0.01185	0.1099
Root mean Square roughness	0.1095	0.1340	0.01512	0.01636	0.1634
Average waviness (W_a)	0.4955	0.6524	0.4927	0.4391	0.4513
Root mean Square waviness	0.7046	0.7842	0.6558	0.5038	0.6039
Skewness	−0.7956	0.4120	0.7759	−0.97	−0.202
Maximum roughness	2.54 µm	0.333 µm	1.28 µm	3.89 µm	0.581 µm

The roughness of all of the nanocomposites' surfaces with falls below 0.2 µm, therefore resist against the bacterial adhesion and hence reducing the risk of plaque accumulation and secondary caries [39]. Further, moderate values of the roughness improve micromechanical interlocking [40].

An obvious decrease in the average and root mean square roughness values for the nanocomposites with 6%, 9% and 12% TiO_2 is observed as compared to the pure PMMA, which leads to lower frictional forces, thereby increases the wear resistance of the restorative nanocomposites. A decrease in average surface roughness enhances the mechanical, biological, and aesthetic performance of dental nanocomposites [39,40]. The incorporation of nanoscale fillers promotes a more uniform surface topography, resulting in reduced average roughness and improved clinical performance. Lowering in surface roughness with increasing TiO_2 content enhances the light reflection, which results in improved gloss and aesthetic appearance and reduces bacterial adhesion and plaque accumulation thereby minimizing the risk of secondary caries [40]. In contrast, the nanocomposite with 3% TiO_2 contents exhibits relatively higher surface roughness, which tends to reduced mechanical strength and increased susceptibility to degradation [19]. The incorporation of nanoscale TiO_2 fillers beyond 3% contributes to a more homogeneous surface morphology, resulting in lower roughness values and improved restorative performance.

Average waviness (W_a) is a critical parameter influencing the functional performance of dental restorative nanocomposites, which represents the average deviation of the surface profile after removing fine

roughness component and predicts the macro-scale surface uniformity. It reveals from the AFM profiles and Table 2, that the nanocomposites with 6%, 9% and 12% TiO_2 filler contents exhibit lowering in the W_a values with filler contents, and the least value is obtained for 9% TiO_2/PMMA nanocomposite. Hence, this nanocomposite exhibits the most uniform surface profile, and offers the enhanced stress distribution, wear resistance, and marginal integrity, thereby has optimized enhanced durability and clinical performance as the dental restorative material [41].

Skewness (Rsk) provides information about the asymmetry of surface height distribution and is an important parameter in dental surface characterization [42]. Surface topography significantly influences the clinical performance of restorative materials, including wear resistance and bacterial adhesion [43,44]. Positive skewness indicates a peak-dominated surface prone to higher wear, whereas negative skewness corresponds to valley-dominated morphology that may improve load distribution. However, surface depressions may also contribute to bacterial retention, affecting long-term durability [44,45]. As clear from the Table 2, all of the samples exhibit negative value of skewness except 3% TiO_2/PMMA nanocomposite, whereas the least negative value (−0.97) is for the TiO_2/PMMA nanocomposite with 9% TiO_2. This confirms the valley-dominated morphology of 9% TiO_2/PMMA nanocomposite, which enhances wear resistance and facilitates saliva retention, improving lubrication as compared to the other nanocomposites reveals a valley dominated morphology, most favorable for load distribution and hence positively influences the material's wear behavior and clinical durability [44].

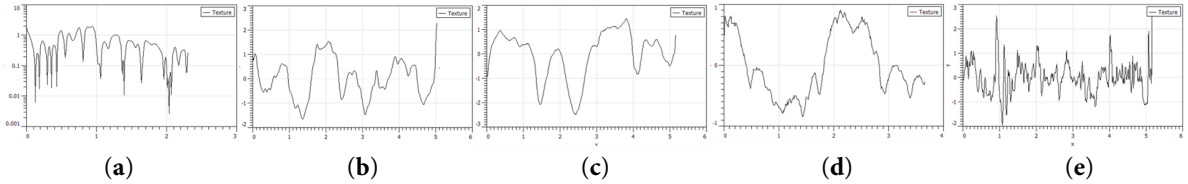

Figure 5: The Texture profile extracted from AFM topographic images (**a**) pure PMMA and TiO_2/PMMA nanocomposites with (**b**) 3%, (**c**) 6%, (**d**) 9% and (**e**) 12% TiO_2.

3.2 Mechanical Properties

3.2.1 Young Modulus, UTM and Break Strength

The mechanical performance of polymer matrix nanocomposites is of essential significance in determining their favorability for dental restorative applications, where the materials are subjected to continuous and complex functional loading. Young's modulus reflects the stiffness of dental restorative materials, which illustrates its ability to resist elastic deformation under applied stress due to reinforcing effect of TiO_2 nanoparticles and restricted mobility of the polymer chains [46]. Likewise, the Ultimate tensile strength (UTS) demonstrates maximum stress, which the material can withstand under uniaxial loading before failure, providing insight into the intrinsic load-bearing capacity of the nanocomposite matrix. However, the break strength denotes the actual load at which fracture occurs and is influenced by the material's integrity, presents a practical indicator of failure resistance under applied force. Flexural strength, evaluated under bending conditions in accordance with ASTM D790, is of particular importance with regards to the dental applications because it simulates masticatory loading and reflects the crack resistance of the nanocomposites and their structural stability under functional oral conditions [47,48].

The mechanical properties of pure PMMA and nanocomposite samples (3%, 6%, 8% and 12%) were evaluated using a universal testing machine (UTM) in tensile mode. A sample of original length 57 mm and

cross-sectional area of 45.50 mm^2 was taken for the test. Young modulus was evaluated by the following Eq. (1) [49];

$$Y = \frac{F.L_o}{A.\Delta L} \quad (1)$$

where F is the tensile force, L_o is the original length of the samples (57 mm), A is the cross-sectional area and ΔL is the elongation. The Young modulus values of pure PMMA and TiO_2/PMMA nanocomposites was evaluated for the initial linear region of the Tensile Force versus Elongation (tensile) curve, presented in Fig. 6a,b.

The tensile curve in Fig. 6a exhibits a linear increase in stress with elongation for pure PMMA, reaching a maximum load of approximately 1400 N, followed by a relatively stable region with minor fluctuations. The Young's modulus of pure PMMA is determined using Eq. (1), which comes out to be 9.11 GPA. The stress-strain behavior of the nanocomposite as shown in Fig. 6b a generally follows a trend similar to that of pure PMMA. However, slight deviations are observed for the nanocomposite with 6% TiO_2 fillers content, indicating possible inconsistencies at lower filler loading.

The values of key mechanical parameters, including Young's modulus, ultimate tensile strength (UTS), and break strength, as extracted from the stress-strain curves, are given in Table 3 below.

The whole data reveal significant enhancement for TiO_2/PMMA nanocomposites in all mechanical properties as compared to the pure PMMA. The Young modulus value shows enhancement of 1.17 times for both PTN-3 and PTN-6, 1.23 for 9% and 1.16 times for PTN-12. Similarly, the ultimate tensile strength (UTS) got enhanced for the nanocomposites, by 2.08 times for PTN-3, 2.24 times for PTN-6, 2.38 times for PTN-9 and 1.78 times for PTN-12. The break strength observes enhancement of 2.15 times for PTN-3, 2.30 times for PTN-6, 2.37 times for PTN-9 and 1.8 times for pTN-12 as compared with the pure PMMA.

Table 3: Values of UTM parameters for PMMA and TiO_2/PMMA nanocomposites.

Sample Name	Young Modulus (GPa)	UTS (MPa)	Break Strength (MPa)	Average Surface Harness (HV)	Average Flexural Strength (MPa)
Pure PMMA	9.11	31.22	30.39	17.22	63.77
PTN-3	10.7	65.20	65.27	35.44	147.69
PTN-6	10.74	69.85	69.8	37.99	154.37
PTN-9	11.21	72.39	72.19	39.23	165.22
PTN-12	10.54	55.5	55.49	39.31	166.11

The variation of mechanical properties (Young's modulus, UTS, and break strength) with increasing TiO_2 content is illustrated in Fig. 7a,b, respectively. All these properties initially increase with the filler loading, and reaches to a maximum value for the nanocomposite with 9 wt% TiO_2, followed by a decline for the nanocomposite with 12% TiO_2 loading. This behavior is attributed to improved dispersion and uniform distribution of TiO_2 nanoparticles within the PMMA matrix at moderate concentrations, which enhances stress transfer. At higher loading (12 wt%), the particle agglomeration and non-uniform distribution likely occur, which lead to the reduced mechanical performance.

3.2.2 Surface Hardness

The surface hardness of PMMA/TiO_2 nanocomposites films was evaluated using the Vickers hardness test. In this test, a diamond indenter with a square-based pyramidal geometry was employed at an angle of 135° between opposite faces. A preset load was applied to the polished surface of the films for a fixed

lodging time (10 s), which results in permanent indentation. Each experiment was performed in triplicate and the results are taken as mean (n = 3).

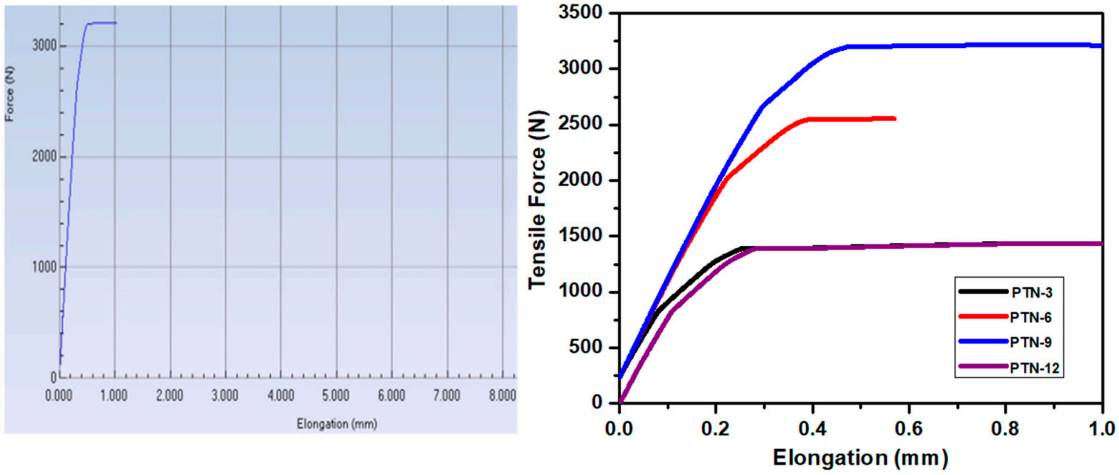

Figure 6: Representative Tensile Force versus Elongation curves for (**a**) pure PMMA and (**b**) PMMA/TiO_2 nanocomposites.

After the load removal, the two diagonals of the indentation were measured using an optical microscope, from which the average diagonal length (d) was found. The Vickers hardness number (HV) was calculated using the following Eq. (2) [50]:

$$HV = \frac{1.854\ F}{d^2} \tag{2}$$

where F denotes applied load and d is the average length of diagonal of indentation. The indentation test was performed with same load 50 g applied at three different locations for all samples and then the mean hardness values were calculated, which are tabulated in Table 3.

Obviously, as shown in Fig. 7c, an increasing trend in hardness value is seen with the increasing TiO_2 fillers contents indicates an enhanced resistance to surface deformation, which is attributed to the reinforcing effect of rigid inorganic fillers within the polymer matrix, leading to improved wear resistance and surface mechanical stability of the nanocomposites for being used as dental restorative materials [51].

3.2.3 Flexural Strength

Flexural strength (or bending strength) is the maximum stress a material can withstand before failure under bending and is determined using a three-point bending test in accordance with ASTM D790 standard [48]. A rectangular film specimen of each sample was placed on two supports at a fixed span length, and a load was applied at the midpoint at a constant crosshead speed until fracture occurred. The Flexural strength was calculated using following Eq. (3) [52]

$$\sigma_F = \frac{3FL}{2bd^2} \tag{3}$$

where F is the applied force, L is the support span, b is the specimen width, and d is the specimen thickness. In this test, the span length (L) was taken as 25 mm and the specimen size of each sample was $1.5 \times 1.5 \times 25\ mm^3$. The crosshead speed was 1 mm/min. Each sample was tested three times, and

the average flexural strength was calculated and is tabulated in Table 3. The results indicate a significant enhancement in flexural strength for the PMMA/TiO_2 nanocomposites as compared to the pure PMMA matrix, with an increase ranging from 2.33 to 2.60 times.

The variation of flexural strength as a function of TiO_2 content is plotted in Fig. 7d. An initial sharp increase in flexural strength was observed with increasing TiO_2 content up to 6 wt%, followed by a plateau region with marginal changes at higher filler loadings. The maximum flexural strength of 166.11 MPa was achieved at 12 wt% TiO_2 content. Notably, the nanocomposites containing 9 wt% and 12 wt% TiO_2 exhibited approximately 2.6 times improvement in flexural strength as compared with pure PMMA. This improvement is attributed to the uniform dispersion of TiO_2 nanoparticles within the polymer matrix and improved interfacial bonding, which facilitates the efficient stress transfer under bending loads [53,54].

From a clinical perspective, increased flexural strength enhances the material's ability to withstand masticatory forces, thereby reducing the risk of fracture and improving the longevity of restorations. The plateau observed beyond 6 wt% TiO_2 suggests that an optimal filler concentration exists, beyond which additional reinforcement yields diminishing returns, likely due to particle agglomeration or reduced matrix continuity. Nevertheless, the substantial improvement at 9 wt% and 12 wt% indicates that TiO_2 reinforcement is effective in producing mechanically robust PMMA-based dental composites suitable for load-bearing applications [53–55].

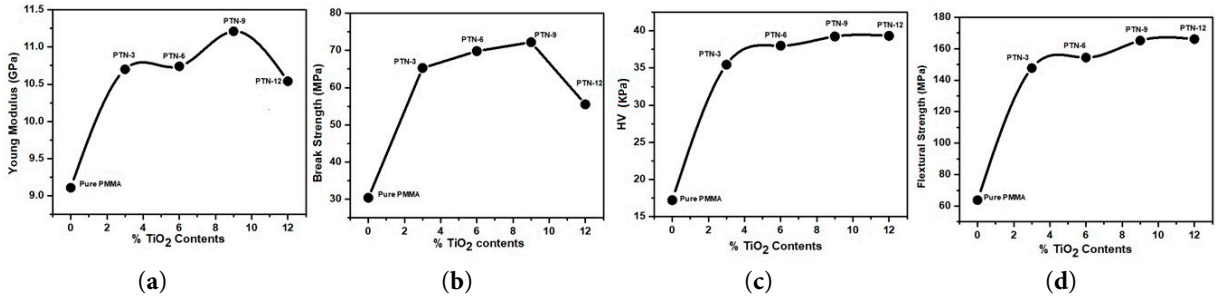

(**a**) (**b**) (**c**) (**d**)

Figure 7: Variation of mechanical properties with % TiO_2 contents (**a**) Young Modulus, (**b**) Break strength, (**c**) Hardness value, and (**d**) Flexural strength.

3.3 Dental Performance Parameters

3.3.1 Water Absorption Test

Water absorption behavior of the samples was evaluated in accordance with ASTM D570 standard [56]. Typically, the sample of small dimensions is immersed in water for a specific period of time and its weight is measured before and after immersing.

The films of pure PMMA and nanocomposites (weighing 120 mg) were immersed in deionized water at room temperature (27 ± 1°C) for 72 h. After which, the samples were taken out and the surface moisture was carefully wiped off prior to final weighing. The percentage weight change was then calculated using Eq. (1).

The water sorption is then calculated using the following relation (4) [57].

$$\% \text{ change in weight} = \frac{\text{Final weight} - \text{initial weight}}{\text{Initial weight}} \times 100 \quad (4)$$

Each sample was tested for three times and average value of the water sorption was calculated accordingly. The percentage water sorption (%WS) for all samples is presented in Fig. 8a. A decreasing trend

in %WS is observed with increasing TiO_2 content up to 9 wt%, as compared with the pure PMMA. A slight upturn is noted for 12% TiO_2 filling. The decrease in water sorption at moderate filler loading is attributed to the improved filler-matrix interaction and reduced free volume within the polymer network. However, at higher TiO_2 loading, possible nanoparticles agglomeration leads to the structural inhomogeneity, resulting in a marginal increase in water absorption. Although PMMA is inherently hydrophobic, the incorporation of TiO_2 nanoparticles contributes to limited water sorption due to their surface characteristics and interaction with the polymer matrix [58,59].

The water absorbed by the dental restorative ingredients compromises the interfacial bonding between the resin matrix and filler particles, thereby diminishing the material's mechanical properties. Consequently, minimizing water sorption is critical for preserving the structural integrity and long-term performance of these materials [1].

3.3.2 Density of the Nanocomposites

Density is a fundamental physical property of the denture base composites, which is determined both before and after curing using the following Eq. (5): [60].

$$\rho = {}^{W_1}/_{W_1 - W_2} \tag{5}$$

where W_1 and W_2 represent the sample weights measured in air and water, respectively. The density of the PMMA used in this study, as specified by the manufacturer, is 1186 Kg/m^3. Table 4 summarizes the experimentally recorded density values in the test.

Table 4: Dental restorative properties (density and %PS) for pure PMMA and nanocomposite samples.

Samples	Density (Kg/m^3)	% Increase in Density	%PS
Pure PMMA	1186	0	10.01
PTN-3	1204	1.5	7.7
PTN-6	1219	2.7	6.4
PTN-9	1240	4.5	5.6
PTN-12	1259	6.1	5.27

Obviously, a slight increase in density is observed for the nanocomposites, which can be attributed to the incorporation of titanium dioxide (TiO_2) nanofillers. This trend is expected, given that the density of TiO_2 (≈4260 Kg/m^3) is significantly higher than that of PMMA. Upon incorporation into the polymer matrix, the resulting nanocomposite exhibits an intermediate density value between those of its constituents (the polymer resin matrix and the filler), with a progressive increase observed as the TiO_2 content increases.

An increase of approximately 4.5% in density is observed for the nanocomposite with 9% TiO_2, without compromising the stability of removable prostheses during mastication, indicating a potentially favorable balance between reinforcement and weight because previous studies have reported that a 5% increase in denture base density is acceptable with the incorporation of 9 wt% nano-sized barium titanate. In general, materials used for denture base fabrication should possess low specific gravity to ensure minimal weight. Increased density is therefore undesirable, particularly for maxillary dentures, as excessive weight may compromise retention and stability, leading to displacement or dislodgement during function.

3.3.3 Polymerization Shrinkage of Nanocomposite

Polymerization shrinkage (PS) is a critical parameter for assessing the dimensional stability of dental restorative materials during curing. The polymerization shrinkage of pure PMMA and TiO_2/PMMA nanocomposites was evaluated by measuring the density of each specimen in both uncured and cured states.

Initially, the uncured samples were weighed in air and in water using an electronic balance, and their densities were calculated by Eq. (5). Subsequently, the samples were heat-cured in a water bath and re-measured following the same procedure. The percentage polymerization shrinkage (%PS) was then determined from the measured densities based on Archimedes' principle, using the following Eq. (6) [61];

$$\%PS = \frac{(\rho_{cured} - \rho_{uncured})}{\rho_{cured}} \times 100 \tag{6}$$

where $\rho_{uncured}$ and ρ_{cured} denote the densities of the uncured and cured specimens in Kg/m^3, respectively. Each sample was repeated for test three times and average values of %PS were calculated, presented in Table 4. The variation of %PS versus % TiO_2 fillers concentration (0% for pure PMMA) is plotted in Fig. 8b.

A pronounced linear decline in %PS is observed in the PMMA/TiO_2 nanocomposites as compared to pure PMMA, which may be explained by filler-matrix interaction mechanisms. Pure PMMA exhibits higher polymerization shrinkage (10.01%) due to extensive conversion of monomer to polymer during the polymerization process, which leads to a reduction in free volume and contraction of the PMMA network. However, upon loading of TiO_2 nanoparticles, a progressive and consistent reduction in %PS is observed (7.7–5.27%), indicating a strong filler-dependent constraint on matrix contraction [53,60].

This significant reduction in %PS (from 23 times to 47 times) is primarily attributed to the "dilution effect," where the incorporation of non-shrinking inorganic TiO_2 nanoparticles decreases the overall volume fraction of polymerizable resin, thereby directly reducing the extent of volumetric contraction during curing. Besides, the TiO_2 nanoparticles act as rigid, high-modulus inclusions, which could restrict the mobility and rearrangement of PMMA polymer chains during polymerization. This restriction reduces the ability of the matrix to undergo densification, thereby limiting shrinkage development [53,62,63].

Polymerization shrinkage in dental resins may also be explained on the basis of two mechanisms: (i) the replacement of relatively weak van der Waals forces between monomer molecules with covalent bonds during polymerization, and (ii) the reduction in intermolecular spacing as monomers are converted into a more compact polymer network [61,64]. These phenomena lead to the development of residual tensile stresses within the material, which can promote interfacial de-bonding between the matrix and filler particles, as well as microleakage [60]. These adverse effects ultimately compromise the mechanical integrity and toughness of the composite. It has been reported that simply increasing filler content is not always sufficient to effectively reduce the overall polymerization shrinkage of composite materials [60,65].

3.4 ANOVA Analysis of Physio-Mechanical Properties

In order to analyze each response (break strength, flexural strength, hardness, water absorption, young's modulus and %PS) with respect to the factor different TiO_2 concentrations, one-way ANOVA (Design-Expert® software, version #13, Stat-Ease, Inc., Minneapolis, MN, USA). The number of replicates is three and their average values are considered with respective standard deviation (σ) for analysis. The results showed that all the responses are statistically significant ($p < 0.05$) at different compositions. The ANOVA results are provided in Table 5 below.

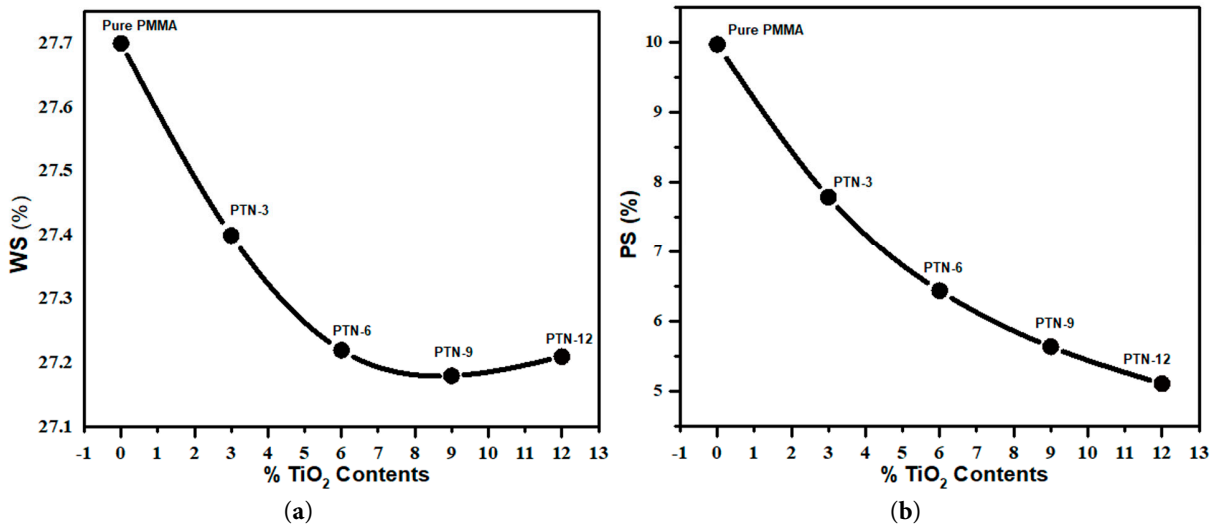

Figure 8: (**a**) Polymerization Shrinkage (PS) and (**b**) Water Sorption in percent for pure PMMA and TiO_2/PMMA nanocomposites.

For break strength property, the determined model is significant (p = 0.036), with high accuracy (R-squared = 96.4%) based on quadratic model, indicating that strength improves up to an optimal filler concentration and then declines. A similar trend is observed in flexural strength, where the quadratic effect dominates (p = 0.0787), indicating a peak performance at intermediate loading despite the overall model showing model accuracy (R-squared = 92.13%). Similarly, water absorption shows a highly significant model (p = 0.0023) with both linear and quadratic terms significant, implying that filler content strongly and systematically influences moisture uptake with model accuracy of 99.77%. For hardness, the model is also significant (p = 0.0362), but the linear term is insignificant (p = 0.7154) while higher-order terms are dominant, confirming that hardness increases nonlinearly with TiO_2 addition. The ANOVA for %PS shows a highly significant effect of TiO_2 content on the response. The overall model is statistically significant (p = 0.0009), demonstrating that the variation in %PS is strongly explained by the change in TiO_2 concentration. Overall, the %PS increases systematically with TiO_2 content, and the effect is both strong and predictable, governed primarily by a linear relationship rather than higher-order interactions. Finally, these results demonstrate that the properties are governed primarily by nonlinear (quadratic/cubic) effects of reinforcement content, reflecting phenomena such as particle dispersion, agglomeration, and interfacial bonding, with optimal performance generally occurring at intermediate filler concentrations rather than at extremes [66,67].

The corresponding responses surface plots to further study the influence of TiO_2 in the nanocomposites (PTN-3, PTN-6, PTN-9 and PTN-12) on the mechanical and physical properties by ANOVA analysis are shown in Fig. 9a–c and Fig. 10a,b, respectively. Fig. 9a,b presents a quadratic effect on break and flexural strength, which reflects enhancement with the TiO_2 contents, reaching to an optimum at intermediate levels (6–9%), and then decrease at a higher loading. This indicates an initial improvement upon reinforcement, followed by deterioration, which might be due to particle agglomeration and stress concentration [68]. Fig. 9c shows a nonlinear increasing trend with a slight saturation, implying that hardness enhances significantly with TiO_2 addition but stabilizes at higher contents due to limited further densification. On the other hand, water absorption shows an inverse relation trend with a slight decrease in absorption at moderate concentrations of TiO_2, and then increases for higher concentrations, as shown in Fig. 10a. Finally, the %PS shows a linear increase with increasing the concentration of TiO_2. All the results are consistent with the ANOVA (Fig. 10b).

Table 5: One way ANOVA results for different physio-mechanical properties of pure PMMA and TiO_2/PMMA nanocomposites with different TiO_2 compositions.

Source	Sum of Squares	df	Mean Square	F-Value	*p*-Value	
Break Strength (σ = 4.57)						
Model	1118.54	2	559.7	26.75	0.0360	significant
A-PTN	326.38	1	326.38	15.61	0.0585	
A^2	792.16	1	792.16	37.88	0.0254	
Residual	41.82	2	20.91			
Cor Total	1160.36	4				
Flexural Strength (σ = 17.04)						
Model	6801.26	2	3400.63	11.71	0.0787	significant
A-PTN	4919.97	1	4919.97	16.94	0.0543	
A^2	1881.29	1	1881.29	6.48	0.01259	
Residual	580.92	2	290.46			
Cor Total	7382.17	4				
Water Absorption (σ = 0.015)						
Model	0.1910	2	0.0955	442.69	0.0023	significant
A-PTN	0.1464	1	0.1464	678.72	0.0015	
A^2	0.0446	1	0.0446	206.66	0.0048	
Residual	0.0004	2	0.0002			
Cor Total	0.1914	4				
Hardness Value (σ = 0.54)						
Model	366.21	3	122.07	411.33	0.0362	significant
A-TiO2	0.0682	1	0.0682	0.2298	0.7154	
A^2	122.93	1	122.93	414.24	0.0313	
A^3	21.17	1	21.17	71.32	0.0750	
Residual	0.2968	1	0.2968			
Cor Total	366.51	4				
%PS (σ = 4.79)						
Model	4080.40	1	4080.40	177.92	0.0009	significant
A-PTN	4080.40	1	4080.40	177.92	0.0009	
Residual	68.80	3	22.93			
Cor Total	4149.20	4				

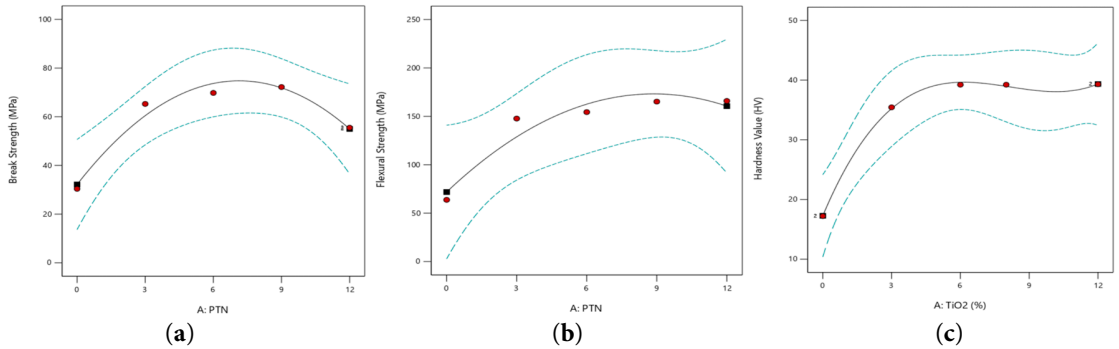

(**a**) (**b**) (**c**)

Figure 9: ANOVA surface plots of the mechanical properties (**a**) Break Strength (**b**) Flexural Strength and (**c**) Hardness Value (HV), for pure PMMA and TiO_2/PMMA nanocomposites.

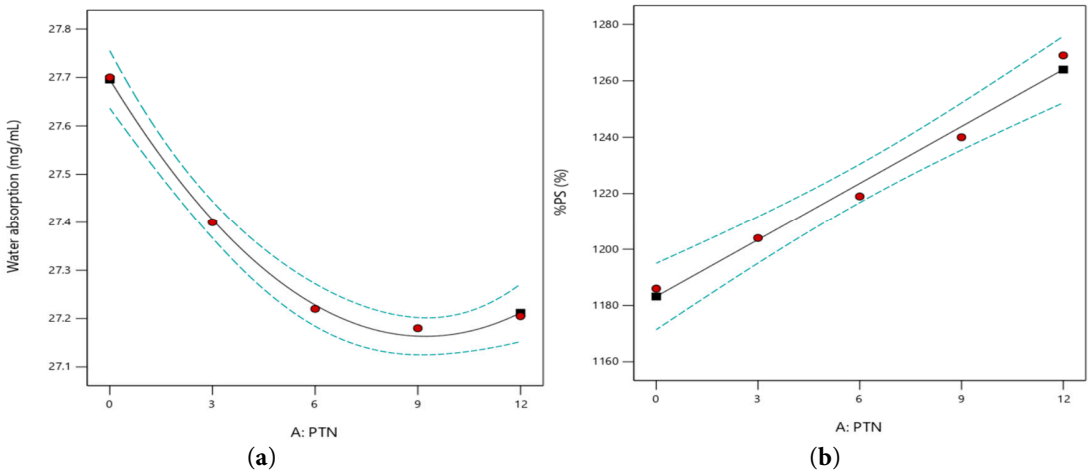

Figure 10: ANOVA surface plots of physical (dental) properties (**a**) Water sorption and (**b**) %PS, for pure PMMA and TiO_2/PMMA nanocomposites.

3.5 Functional Groups Analysis by Fourier Transform Infra-Red (FTIR) Spectroscopy and Enhancement in Physio-Mechanical Properties

The Fourier Transform Infrared (FTIR) spectroscopy of pure PMMA and TiO_2/PMMA nanocomposites was performed to examine the chemical structure and interfacial interactions present in the PMMA/TiO_2 nanocomposites. Fig. 11a–c presents the FTIR spectra profiles of Pure PMMA and TiO_2/PMMA nanocomposites and corresponding bands occurring with their intensities are given in Table 6. The FTIR spectrum of pure PMMA film (Fig. 11a) exhibits characteristic absorption bands corresponding to its functional groups such that a strong absorption peak is observed at 1714.57 cm^{-1}, which is attributed to the stretching vibration of the ester carbonyl (C=O) group, thereby confirming the presence of the methacrylate backbone [69]. Similarly, the peaks occurring in the range 1297.11 cm^{-1} correspond to C-O-C stretching vibrations, while bands lying in the region of 2959.51 cm^{-1} are assigned to the asymmetric and symmetric stretching of -CH_3 and -CH_3 groups [70]. Furthermore, a weak band at ~1450 cm^{-1} is associated with the bending vibrations of methyl groups [71]. Additionally, two peaks occurring at 2027.91 and 2160.17 cm^{-1} (2000–2500 cm^{-1}), are observed, showing atmospheric CO_2 absorption, having asymmetric stretching vibration, might be due to poor background subtraction or instrumental environment [72].

However, the FTIR spectra of PMMA/TiO_2 nanocomposites, as shown in Fig. 11b present considerable changes upon incorporation of TiO_2 nanoparticles and some additional features and subtle spectral shifts are observed, which obviously indicate the interactions between PMMA matrix and TiO_2 nanofillers. The magnified FTIR spectra of nanocomposites (Fig. 11c) obviously show the occurrence of bands appearing in the range ~400–700 cm^{-1}, assigned to Ti-O-Ti stretching vibrations, thereby confirming the successful incorporation of TiO_2 within the PMMA matrix [73] and imparts anti-bacterial properties thereby reducing microbial colonization and improving clinical performance. Similarly, the preservation of hydrophobic nature of alkyl groups (–CH_3 and –CH_2) in the nanocomposites contributes to reduced water sorption, thereby enhancing dimensional stability in the moist oral environment [73].

Furthermore, as seen in the Fig. 9b, slight average shift in the carbonyl (C=O) band toward lower wavenumbers (0.7% for PTN-3, 2.39% for PTN-6), 0.21% for PTN-9 and 0.46% for PTN-12) suggests possible coordination or hydrogen bonding interactions between the oxygen of the ester group and the surface hydroxyl groups of TiO_2 nanoparticles. The intensity variation and minor broadening of peaks in the 3200–3500 cm^{-1} range indicates the presence of hydroxyl (-OH) groups, likely to be originating from

adsorbed moisture or surface hydroxylation of TiO_2 [65,69], which looks relatively more visible in PTN-9. These hydroxyl groups are responsible to facilitate the interfacial adhesion between the inorganic TiO_2 filler and the organic PMMA matrix. The two peaks occurring at 2027.91 and 2160.17 cm^{-1}, corresponding to CO_2 absorption also appears in the nanocomposites.

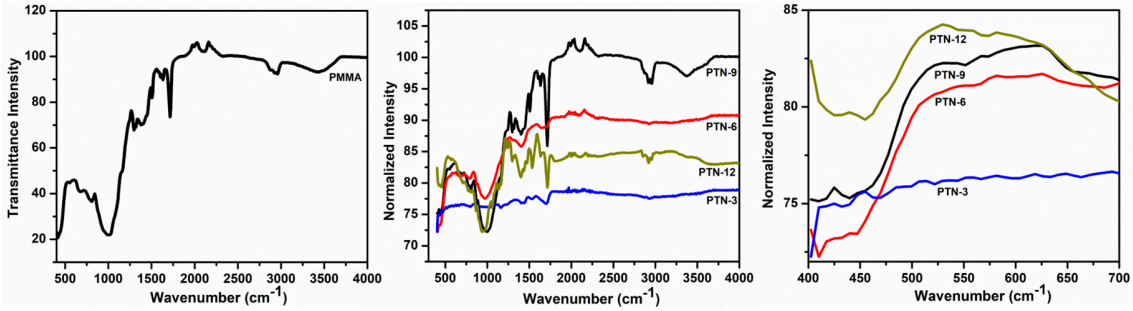

Figure 11: FTIR spectrum of (**a**) Pure PMMA and (**b**) TiO_2/PMMA nanocomposites, (**c**) Magnified FTIR spectrum of TiO_2/PMMA nanocomposites in the 400–700 cm^{-1} range.

Table 6: Observed bands in the FTIR spectrum of Pure PMMA and TiO_2/PMMA nanocomposites with corresponding intensities.

PMMA		PTN-3		PTN-6		PTN-9		PTN-12	
Wave Number (cm^{-1})	Intensity (cps)	Wave Number (cm^{-1})	Intensity (cps)	Wave Number (cm^{-1})	Intensity (cps)	Wave Number (cm^{-1})	Intensity (cps)	Wave Number (cm^{-1})	Intensity (cps)
805.10	63.64	437.33	75.07	410.72	72.71	435.50	75.99	454.24	79.81
984.02	53.66	805.10	79.01	443.73	73.86	1036.20	97.01	454.73	95.78
1297.11	82.34	998.93	72.25	685.83	90.23	1162.93	96.92	939.29	87.21
1401.48	83.28	1297.11	88.08	790.19	89.94	1408.93	97.86	1058.56	91.86
1505.84	91.19	1401.48	87.74	969.11	86.39	1535.66	98.71	1133.11	95.31
1714.57	84.25	1505.84	91.41	1401.48	95.59	1699.67	97.73	1706.58	79.44
2959.51	95.45	1702.34	76.93	1673.05	86.05	1710.97	85.99	3712.43	100
3444.06	96.09	2952.05	95.83						
		3369.51	97.02						

3.6 Performance Mechanism Based on Interfacial Chemistry

The performance of TiO_2/PMMA nanocomposites as dental restorative materials and the promising nature of 9% TiO_2 contents as an optimized fillers content may be well explained on the basis of interfacial chemistry analysis. Molecular-level interactions as identified through FTIR analysis are firmly responsible for the improved physicochemical and functional properties of PMMA/TiO_2 nanocomposites. The FTIR spectra reveal the presence of interfacial interactions primarily through hydrogen bonding and possible coordination with carbonyl groups. Such interactions contribute to the enhancement of physicochemical and mechanical properties by nanocomposite, making them favorable for dental restoration purposes, because of having improved strength, durability, and resistance to the microbial activity [74]. The ester carbonyl (C=O) groups contribute significantly to the rigidity and structural integrity of polymer PMMA and its interaction with the TiO_2 nanofillers. Leading to interfacial bonding, which results in improved mechanical properties including flexural strength, wear resistance, etc. Likewise, the preservation of C-O-C bands demonstrates that the polymer mainstay remains chemically stable even after the TiO_2 incorporation,

which ensures biocompatibility and long-term durability in oral conditions [75]. As clear from the Table 6, the average intensity of all bands is high for the PTN-9 nanocomposite among all nanocomposites.

4 Conclusions

In this work, TiO2/PMMA nanocomposites with distinct wt% TiO2 nanofillers (3%, 6%, 9%, and 12%) were successfully prepared via a combinatory hydrothermal-solvothermal approach. The prepared nanocomposites were characterized and compared with pure PMMA in terms of their structural, surface morphology/roughness, and functional groups using X-ray diffraction (XRD), Atomic Force Microscopy (AFM), and Fourier Transform Infrared (FTIR) spectroscopy, respectively. The physio-mechanical properties, including Young modulus, ultimate tensile strength, break strength, hardness value (HV), flexural strength, water absorption, density tests, and polymerization shrinkage, were measured using UTM, ASTM D790 standard, the Archimedes method, and ASTM D570 standard, respectively. Structural analysis confirmed the successful incorporation of TiO2 nanoparticles within the PMMA matrix. AFM analysis demonstrated a uniform dispersion of TiO2 nanoparticles throughout the PMMA matrix and showed the surface roughness of all nanocomposites below 0.2 μm with negative skewness. FTIR shows spectral shifts for nanocomposites, which obviously indicate the interactions between the PMMA matrix and TiO2 nanofillers. The Young's modulus, ultimate tensile strength, break strength, hardness value (HV) and flexural strength of the nanocomposites revealed significant enhancement as compared with that of pure PMMA such that optimized values (1.23 times or 23% in Young modulus, 2.38 times in UTS, 2.37 times in break strength and more than 2 times in HV) are achieved for the nanocomposite with 9 wt% TiO2. The flexural strength of the nanocomposites revealed a 2.33–2.60 times enhancement as compared with the baseline value (63.77 for pure PMMA), reaching up to 166.11 MPa at higher TiO2 loadings (9–12 wt%). The water absorption behavior of nanocomposites presented a linear monotonic decrease up to 9% TiO2 loading, followed by a slight increase afterwards. Furthermore, polymerization shrinkage (%PS) exhibited a pronounced linear decrease (47–52%) for the nanocomposites as compared to pure PMMA. ANOVA analysis of all of the physio-mechanical properties confirms their statistical significance at different compositions. Conclusively, among all the prepared samples, the nanocomposite containing 9 wt% TiO2 exhibited an optimized physio-mechanical performance, highlighting it as a potential candidate as a dental restorative material, which has been explained on the basis of interfacial chemistry. However, its cytotoxicity, antibacterial, and bioactivity assessments may be performed prior to establishing its biocompatibility and clinical relevance.

Acknowledgement: The technical support of Dental unit of Khyber Medical University, Peshawar for carrying out the samples' curing and other analysis, is highly acknowledged.

Funding Statement: This work is jointly supported by Higher Education Commission of Pakistan vide its Project No. NRPU #17387 and Princess Nourah bint Abdulrahman University Researchers Supporting Project number (PNURSP2026R398), Princess Nourah bint Abdulrahman University, Riyadh, Saudi Arabia which are highly acknowledged.

Author Contributions: The authors confirm contribution to the paper as follows: Conceptualization, methodology, resources, project administration, supervision, writing original draft, AFM software analysis: Abdul Hakim Shah; Methodology, data collection: Hassan Khan; Resources, writing original draft, AFM software analysis, editing of revised draft: Muneerah Alomar; Co-supervision: Atta ur Rahman; ANOVA analysis, Data curation: Muhammad Hanif; Characterization and validation of dental restorative properties: Salah ud Din; Investigation, and analysis: Haseena Riffat; Writing of revised draft: Nazir ur Rehman; FTIR characterization and validation: Munazza Gul; Investigation, Visualization: Muhammad Danyal Zarin; Data collection, investigation: Muhammad Faran; Data collection, analysis: Muhammad Wasim; Investigation, Visualization: Aqib Umar. All authors reviewed and approved the final version of the manuscript.

Availability of Data and Materials: The data that support the findings of this study are available from the Corresponding Author, Abdul Hakim Shah, upon reasonable request.

Ethics Approval: Not applicable.

Conflicts of Interest: The authors declare no conflicts of interest.

References

1. Wu M, Zhang F, Yu J, Zhou H, Zhang D, Hu C, et al. Fabrication and evaluation of light-curing nanocomposite resins filled with surface-modified TiO_2 nanoparticles for dental application. Iran Polym J. 2014;23(7):513–24. [CrossRef].
2. Selwitz RH, Ismail AI, Pitts NB. Dental caries. Lancet. 2007;369(9555):51–9. [CrossRef].
3. Kim JW, Kim LU, Kim CK. Size control of silica nanoparticles and their surface treatment for fabrication of dental nanocomposites. Biomacromolecules. 2007;8(1):215–22.
4. Liu Y, Tan Y, Lei T, Xiang Q, Han Y, Huang B. Effect of porous glass–ceramic fillers on mechanical properties of light-cured dental resin composites. Dent Mater. 2009;25(6):709–15. [CrossRef].
5. Wang H, Zhu M, Li Y, Zhang Q, Wang H. Mechanical properties of dental resin composites by co-filling diatomite and nanosized silica particles. Mater Sci Eng C. 2011;31(3):600–5. [CrossRef].
6. Miao X, Zhu M, Li Y, Zhang Q, Wang H. Synthesis of dental resins using diatomite and nano-sized SiO_2 and TiO_2. Prog Nat Sci Mater Int. 2012;22(2):94–9. [CrossRef].
7. Balaji S, Ajay R, Deepa G, Muthamilselvi M, Vasanthakumari A, Sonia A. Synthesis and characterization of a chemico-structurally modified bis-GMA analog for dental applications. J Contemp Dent Pract. 2024;25(6):588–92. [CrossRef].
8. Cedillo J, Domínguez AJ, Espinosa JR. Bioactive materials in restorative dentistry. RODYB. 2021;10(3):19–29. [CrossRef].
9. François P, Remadi A, Le Goff S, Abdel-Gawad S, Attal JP, Dursun E. Flexural properties and dentin adhesion in recently developed self-adhesive bulk-fill materials. J Oral Sci. 2021;63(2):139–44. [CrossRef].
10. Sajjad M, Feichtenschlager B, Pabisch S, Svehla J, Koch T, Seidler S, et al. Study of the effect of the concentration, size and surface chemistry of zirconia and silica nanoparticle fillers within an epoxy resin on the bulk properties of the resulting nanocomposites. Polym Int. 2012;61(2):274–85. [CrossRef].
11. Alsharif SO, Bin Md Akil H, Abbas Abd El-Aziz N, Arifin Bin Ahmad Z. Effect of alumina particles loading on the mechanical properties of light-cured dental resin composites. Mater Des. 2014;54:430–5. [CrossRef].
12. Sidhu S, Nicholson J. A review of glass-ionomer cements for clinical dentistry. J Funct Biomater. 2016;7(3):16. [CrossRef].
13. Sun J, Jiang J, Huang Z, Ma X, Shen T, Pan J, et al. Smart biomaterials in restorative dentistry: recent advances and future perspectives. Mater Today Bio. 2025;35:102349. [CrossRef].
14. Abdulrazzaq Naji S, Behroozibakhsh M, Jafarzadeh Kashi TS, Eslami H, Masaeli R, Mahgoli H, et al. Effects of incorporation of 2.5 and 5 wt% TiO_2 nanotubes on fracture toughness, flexural strength, and microhardness of denture base poly methyl methacrylate (PMMA). J Adv Prosthodont. 2018;10(2):113–21. [CrossRef].
15. Gungor H, Gundogdu M, Alkurt M, Yesil Duymus Z. Effect of polymerization cycles on flexural strengths and microhardness of different denture base materials. Dent Mater J. 2017;36(2):168–73. [CrossRef].
16. Kango S, Kalia S, Celli A, Njuguna J, Habibi Y, Kumar R. Surface modification of inorganic nanoparticles for development of organic–inorganic nanocomposites—a review. Prog Polym Sci. 2013;38(8):1232–61. [CrossRef].
17. Qian C, Zhang XY, Zhu BS, Lin KL, Chang J, Zhang XJ. The effect of $CaSiO_3$Nano-particles reinforced denture polymethyl methacrylate. Adv Compos Lett. 2011;20:096369351102000102. [CrossRef].
18. Kuan HC, Ma CM, Chang WP, Yuen SM, Wu HH, Lee TM. Synthesis, thermal, mechanical and rheological properties of multiwall carbon nanotube/waterborne polyurethane nanocomposite. Compos Sci Technol. 2005;65(11–12):1703–10. [CrossRef].
19. Azmy E, Al-Kholy MRZ, Al-Thobity AM, Gad MM, Helal MA. Comparative effect of incorporation of ZrO(2), TiO_2, and SiO_2 nanoparticles on the strength and surface properties of PMMA denture base material: an *in vitro* study. Int J Biomater. 2022;2022:5856545. [CrossRef].

20. Sodagar A, Kassaee MZ, Akhavan A, Javadi N, Arab S, Kharazifard MJ. Effect of silver nano particles on flexural strength of acrylic resins. J Prosthodont Res. 2012;56(2):120–4. [CrossRef].
21. Skovgaard M, Almdal K, Sørensen BF, Linderoth S, van Lelieveld A. Shrinkage reduction of dental composites by addition of expandable zirconia filler. J Compos Mater. 2011;45(26):2817–22. [CrossRef].
22. Gad MM, Al-Thobity AM, Rahoma A, Abualsaud R, Al-Harbi FA, Akhtar S. Reinforcement of PMMA denture base material with a mixture of ZrO(2) nanoparticles and glass fibers. Int J Dent. 2019;2019:2489393. [CrossRef].
23. Yu B, Ahn JS, Lim JI, Lee YK. Influence of TiO_2 nanoparticles on the optical properties of resin composites. Dent Mater. 2009;25(9):1142–7. [CrossRef].
24. Asar NV, Albayrak H, Korkmaz T, Turkyilmaz I. Influence of various metal oxides on mechanical and physical properties of heat-cured polymethyl methacrylate denture base resins. J Adv Prosthodont. 2013;5(3):241–7. [CrossRef].
25. Lin H, Yin X, Wang Z, Xu J, Wang Y, Cheng S, et al. Friction-induced PTFE coating on dental restorative resin with ultralow friction and wear. Langmuir. 2025;41(33):22501–6.
26. Guo X, Li J, Wu Y, Xu L. Recent advancements in hydrogels as novel tissue engineering scaffolds for dental pulp regeneration. Int J Biol Macromol. 2024;264(Pt 2):130708. [CrossRef].
27. Wu M, Xu L, Xing F, Xiao R, Wu W. Novel self-setting cements based on tricalcium silicate/(β-tricalcium phosphate/monocalcium phosphate anhydrous)/hydroxypropyl methylcellulose: from hydration mechanism to biological evaluations. Int J Biol Macromol. 2024;267(Pt 1):131580. [CrossRef].
28. Hao X, Jiang B, Wu J, Xiang D, Xiong Z, Li C, et al. Nanomaterials for bone metastasis. J Control Release. 2024;373:640–51. [CrossRef].
29. Zhang L, Zhang H. Ti-based metallic glass composites containing β-Ti dendrites. Prog Mater Sci. 2025;152:101472. [CrossRef].
30. Babakhani A, AzamiGheimasi S. Preparing self-cleaning and antibacterial polysulfone nano-fibers using TiO_2, ZnO, and SiO_2 nanoparticles with electrospinning method. Invent Discl. 2023;3:100015. [CrossRef].
31. Kunrath MF, Farina G, Sturmer LBS, Teixeira ER. TiO_2 nanotubes as an antibacterial nanotextured surface for dental implants: systematic review and meta-analysis. Dent Mater. 2024;40(6):907–20. [CrossRef].
32. Han X, Chen Y, Jiang Q, Liu X, Chen Y. Novel bioactive glass-modified hybrid composite resin: mechanical properties, biocompatibility, and antibacterial and remineralizing activity. Front Bioeng Biotechnol. 2021;9:661734. [CrossRef].
33. Li SQ, Zhu RR, Zhu H, Xue M, Sun XY, Yao SD, et al. Nanotoxicity of TiO_2 nanoparticles to erythrocyte *in vitro*. Food Chem Toxicol. 2008;46(12):3626–31. [CrossRef].
34. Zhang X, Zhang YC, Wang HR, Xu DD, Li HY, Zhang M. The application of hydrothermal and solvothermal methods in preparing materials. Adv Ceram. 2024;45(3):247–58.
35. Fu G, Vary PS, Lin CT. Anatase TiO_2 nanocomposites for antimicrobial coatings. J Phys Chem B. 2005;109(18):8889–98. [CrossRef].
36. Watson SS, Beydoun D, Scott JA, Amal R. The effect of preparation method on the photoactivity of crystalline titanium dioxide particles. Chem Eng J. 2003;95(1–3):213–20. [CrossRef].
37. Hashem M, Rez MF, Fouad H, Elsarnagawy T, Elsharawy M, Umar A, et al. Influence of titanium oxide nanoparticles on the physical and thermomechanical behavior of poly methyl methacrylate (PMMA): a denture base resin. Sci Adv Mater. 2017;9(6):938–44. [CrossRef].
38. Kawsar M, Hossain MS, Bahadur NM, Ahmed S. Synthesis of nano-crystallite hydroxyapatites in different media and a comparative study for estimation of crystallite size using Scherrer method, Halder-Wagner method size-strain plot, and Williamson-Hall model. Heliyon. 2024;10(3):e25347. [CrossRef].
39. AlGhamdi MA, Fouda SM, Al-Dulaijan YA, Khan SQ, El Zayat M, Al Munif R, et al. Nanocomposite 3D printed resins containing titanium dioxide (TiO_2) nanoparticles: an *in vitro* analysis of color, hardness, and surface roughness properties. Front Dent Med. 2025;6:1581461. [CrossRef].
40. Altarazi A, Haider J, Alhotan A, Silikas N, Devlin H. 3D printed denture base material: the effect of incorporating TiO_2 nanoparticles and artificial ageing on the physical and mechanical properties. Dent Mater. 2023;39(12):1122–36. [CrossRef].
41. Arf AN, Kareem FA, Gul SS. Influence of nanoparticle dispersion on surface morphology and roughness of PMMA-based nanocomposites. Polymers. 2023;15(6):1479. [CrossRef].

42. Duboust N, Ghadbeigi H, Pinna C, Ayvar-Soberanis S, Collis A, Scaife R, et al. An optical method for measuring surface roughness of machined carbon fibre-reinforced plastic composites. J Compos Mater. 2017;51(3):289–302. [CrossRef].
43. Sheikh-Ahmad JY. Mechanics of chip formation. In: Machining of polymer composites. Boston, MA, USA: Springer; 2009. p. 63–110. [CrossRef].
44. Bilgili D, Dündar A, Barutçugil Ç, Tayfun D, Özyurt ÖK. Surface properties and bacterial adhesion of bulk-fill composite resins. J Dent. 2020;95:103317. [CrossRef].
45. Isabel CAC, Dominguette AAS, dos Santos SG, Ribeiro JCR, Moysés MR. Surface roughness of a resin composite. RGO Rev Gaúch Odontol. 2016;64(1):50–5. [CrossRef].
46. Sun F, Zhang J, Liu T, Yao H, Wang L, Meng H, et al. A versatile microporous design toward toughened yet softened self-healing materials. Adv Mater. 2024;36(50):e2410650. [CrossRef].
47. Xu D, Zhang S, Qin Y. Study of the micromechanical properties and dissolution characteristics of porous coral reef limestone. JGR Solid Earth. 2024;129(11):e2024JB029131. [CrossRef].
48. Ivorra-Martinez J, Ferrer I, Aguado R, Delgado-Aguilar M, Garcia-Romeu ML, Boronat T. Development of P(3HB-co-3HHx) nanohydroxyapatite (nHA) composites for scaffolds manufacturing by means of fused deposition modeling. Int J Bioprinting. 2024;10(1):156. [CrossRef].
49. Williams H. Measuring Young's modulus with a tensile tester. Phys Educ. 2022;57(2):025016. [CrossRef].
50. Tayeb HK, Silikas N, Alhaddad AJ, Satterthwaite J. Flexural strength and hardness analysis of 3D-printed vs. milled resin composites indicated for definitive crowns. J Funct Biomater. 2025;16(12):468. [CrossRef].
51. Ferracane JL. Resin composite—state of the art. Dent Mater. 2011;27(1):29–38. [CrossRef].
52. Chander NG, Jayaraman V, Sriram V. Comparison of ISO and ASTM standards in determining the flexural strength of denture base resin. Eur Oral Res. 2019;53(3):137–40. [CrossRef].
53. Sodagar A, Bahador A, Khalil S, Saffar Shahroudi A, Zaman Kassaee M. The effect of TiO_2 and SiO_2 nanoparticles on flexural strength of poly (methyl methacrylate) acrylic resins. J Prosthodont Res. 2013;57(1):15–9. [CrossRef].
54. Rahman IA, Padavettan V. Synthesis of silica nanoparticles by sol-gel: size-dependent properties, surface modification, and applications in silica-polymer nanocomposites—a review. J Nanomater. 2012;2012:132424. [CrossRef].
55. Lekrine JA, Belaadi JA, Boumaaza JM, Alshahrani JH, Bourchak JM. Water absorption of industrial high-density polyethylene biocomposites reinforced with Washingtonia filifera fibers: optimization using Fick's RSM and ANN models [Internet]. 2022 [cited 2026 Jan 1]. Available from: https://www.researchsquare.com/article/rs-1538795/v1.
56. Kormin S, Kormin F, Beg MH. Study on the biodegradability and water adsorption of ldpe/sago starch blend. J Phys Conf Ser. 2019;1150:012033. [CrossRef].
57. Ali Sabri B, Satgunam M, Abreeza N, N Abed A. A review on enhancements of PMMA denture base material with different nano-fillers. Cogent Eng. 2021;8(1):1875968. [CrossRef].
58. Alwan SA, Alameer SS. The effect of the addition of silanized nano titania fillers on some physical and mechanical properties of heat cured acrylic denture base materials. J Baghdad Coll Dent. 2015;27(1):86–91. [CrossRef].
59. Elshereksi NW, Muchtar A, Azhari CH. Effects of nanobarium titanate on physical and mechanical properties of poly(methyl methacrylate) denture base nanocomposites. Polym Polym Compos. 2021;29(5):484–96. [CrossRef].
60. Wang R, Zhang M, Liu F, Bao S, Wu T, Jiang X, et al. Investigation on the physical-mechanical properties of dental resin composites reinforced with novel bimodal silica nanostructures. Mater Sci Eng C Mater Biol Appl. 2015;50:266–73. [CrossRef].
61. Gad MM, Fouda SM, Al-Harbi FA, Näpänkangas R, Raustia A. PMMA denture base material enhancement: a review of fiber, filler, and nanofiller addition. Int J Nanomed. 2017;12:3801–12. [CrossRef].
62. Musanje L, Ferracane JL. Effects of resin composition and filler size on polymerization shrinkage and mechanical properties of restorative composites. Dent Mater. 2004;20(6):519–31. [CrossRef].
63. Ilie N, Hickel R. Investigations on a methacrylate-based composite material. Clin Oral Investig. 2009;13:427–35. [CrossRef].
64. Luo S, Liu F, Yu B, He J. Preparation of low shrinkage stress Bis-GMA free dental resin composites with a synthesized urethane dimethacrylate monomer. J Biomater Sci Polym Ed. 2019;30(2):137–49. [CrossRef].

65. de Carvalho Panzeri Pires de Souza F, Drubi Filho B, Casemiro LA, da Fonseca Roberti Garcia L, Consani S. Polymerization shrinkage stress of composites photoactivated by different light sources. Braz Dent J. 2009;20(4):319–24. [CrossRef].
66. Lu Y, Qi S, Zhang H, Wang Y, You W, Bian F, et al. Structures and dynamics of polymer nanocomposites: filler-polymer interaction and desorption-mediated agglomeration. Polymer. 2026;346:129627. [CrossRef].
67. Sharma SK, Sharma LK, Pradhan R, Sharma Y, Sharma M, Gajević S, et al. Interphase-centric and mechanism-driven advances in polymer composites reinforced with nano-, synthetic, and inorganic fillers. Polymers. 2026;18(3):323. [CrossRef].
68. Abhiram BR, Ghosh D. Influence of nanofiller agglomeration on fracture properties of polymer nanocomposite: insights from atomistic simulation. Eng Fract Mech. 2023;290:109503. [CrossRef].
69. Rajakumar G, Rahuman AA, Roopan SM, Khanna VG, Elango G, Kamaraj C, et al. Fungus-mediated biosynthesis and characterization of TiO_2 nanoparticles and their activity against pathogenic bacteria. Spectrochim Acta A Mol Biomol Spectrosc. 2012;91:23–9. [CrossRef].
70. Vijayakumari G, Selvakumar N, Jeyasubramanian K, Mala R. Investigation on the electrical properties of polymer metal nanocomposites for physiological sensing applications. Phys Procedia. 2013;49:67–78. [CrossRef].
71. Melo-Soares V, dos Reis AC, Valente MLC. Optimizing titanium dioxide-functionalized PMMA for dental applications. Jpn Dent Sci Rev. 2025;61:236–49. [CrossRef].
72. Ahmed W, Osborne EL, Veluthandath AV, Senthil Murugan G. A rapid and simplified approach to correct atmospheric absorptions in infrared spectra. Anal Chem. 2024;96(45):18052–60. [CrossRef].
73. Mansoor A, Mehmood M, Ishtiaq M, Jamal A. Synthesis of TiO_2 nanoparticles and demonstration of their antagonistic properties against selected dental caries promoting bacteria. Pak J Med Sci. 2023;39(5):1249–54. [CrossRef].
74. Yadfout A, Asri Y, Merzouk N, Regragui A. Denture base resin coated with titanium dioxide (TiO_2): a systematic review. Int J Nanomed. 2023;18:6941–53. [CrossRef].
75. Gupta A, Kumari S, Avinashi SK, Mishra RK, Kumar R, Behera P, et al. Influence of TiO_2 as a filler into PMMA-ZrO_2 composites on structural, mechanical and biological properties for denture fabrication. Ceram Int. 2025;51(29):61811–32. [CrossRef].